NANOMATERIALS

Curvature-guided depletion stabilizes Kagome superlattices of nanocrystals

Siyu Wan[1]†, Xiuyang Xia[2]†‡, Yutong Gao[1], Heyang Zhang[1], Zhebin Zhang[3], Fangyue Wu[1], Xuesong Wu[1], Dong Yang[3], Tongtao Li[1]*, Jianfeng Li[3]*, Ran Ni[2]*, Angang Dong[1]*

Shape-anisotropic nanocrystals and patchy particles have been explored to construct complex superstructures, but most studies have focused on convex shapes. We report that nonconvex, dumbbell-shaped nanocrystals (nanodumbbells) exhibit globally interlocking self-assembly behaviors governed by curvature-guided depletion interactions. By tailoring the local curvature of nanodumbbells, we can precisely and flexibly adjust particle bonding directionality, a level of control rarely achievable with conventional convex building blocks. These nanodumbbells can undergo long-range ordered assembly into various intricate two-dimensional superlattices, including the chiral Kagome lattice. Theoretical calculations reveal that the Kagome lattice is a thermodynamically stable phase, with depletion interactions playing a crucial role in stabilizing these non–close-packed structures. The emergence of Kagome lattices and other unusual structures highlights the vast potential of nonconvex nanocrystals for creating sophisticated architectures.

A long-standing goal in the field of colloidal assembly is to create synthetic superstructures that mimic or even surpass the structural complexity found in natural materials (*1*–*6*). Self-assembly of colloidal nanocrystals (NCs) into superlattices provides a programmable approach to developing metamaterials with tailored optical, electronic, and catalytic properties (*7*–*9*). Achieving this requires precise control over the directionality of particle bonding, akin to the specificity observed in molecular synthesis (*10*, *11*). This level of control is particularly important for designing intricate structures such as low-symmetry, low-density lattices, which rely on highly specific and directional interparticle interactions (*12*). However, most NCs studied to date have simple convex shapes, such as spheres and polyhedral. Such high symmetry inherently limits the extent to which directional interactions can be manipulated (*13*, *14*). Surface modifications, such as generating patchiness through site-specific functionalization (*15*–*17*), can enhance interaction specificity, but attaining the desired surface characteristics is challenging. To achieve the rational design of sophisticated architectures, it is essential to develop new design principles that enable NCs to selectively recognize and flexibly bond with neighboring particles.

[1]Department of Chemistry and Shanghai Key Laboratory of Molecular Catalysis and Innovative Materials, iChEM, Fudan University, Shanghai, China. [2]School of Chemistry, Chemical Engineering and Biotechnology, Nanyang Technological University, Singapore, Singapore. [3]State Key Laboratory of Molecule Engineering of Polymers and Department of Macromolecular Science, Fudan University, Shanghai, China. *Corresponding author. Email: agdong@fudan.edu.cn (A.D.); r.ni@ntu.edu.sg (R.N.); lijf@fudan.edu.cn (J.L.); ttli@fudan.edu.cn (T.L.)
†These authors contributed equally to this work.
‡Present address: Arnold Sommerfeld Center for Theoretical Physics and Center for NanoScience, Department of Physics, Ludwig-Maximilians-Universität München, Munich, Germany.

This study introduces nonconvex NCs, specifically nanodumbbells (NDs), as versatile building blocks that offer specific and flexible control over directional interactions through local concave-convex curvature matching. Additionally, we demonstrate that introducing depletion interactions is essential for facilitating the long-range interlocking assembly of NDs, resulting in the formation of diverse and intricate two-dimensional (2D) superlattices. These include non–close-packed architectures such as the Kagome lattice, a structure of interest in condensed-matter physics and materials science (*18*, *19*), yet notoriously challenging to create with conventional convex building blocks (*20*).

Synthesis and characterization of NDs

The NDs that we used were colloidal $NaYF_4$:Yb/Er@$NaGdF_4$@$NaNdF_4$ NCs, synthesized following a reported method (fig. S1) (*21*). The as-synthesized NDs were coated with oleic acid ligands, ensuring their high colloidal stability when dispersed in nonpolar solvents such as hexane (fig. S2). Transmission electron microscopy (TEM) tomography revealed that each ND comprised two convex heads connected by a concave waist (Fig. 1A and movie S1), and high-resolution TEM (HRTEM, Fig. 1B) and wide-angle electron diffraction (WAED, Fig. 1C) confirmed its single-crystalline nature. By optimizing synthetic conditions, we could widely tune the waist width (d) of NDs while keeping the length (L) and head width (D) relatively constant at 60 ± 8 nm and 40 ± 7 nm, respectively. We defined the concavity of NDs using the waist-to-head width ratio (d/D), with a higher ratio corresponding to reduced concavity. This parameter, continuously adjustable between 0.4 and 0.9 (fig. S3), crucially influenced the self-assembly behavior of NDs.

The selection of these NDs as nonconvex building blocks was primarily motivated by their geometric self-complementarity. Figure 1D presents the TEM images of three representative ND shapes, named ND-1, ND-2, and ND-3, corresponding to high, moderate, and low concavity, with d/D ratios of ~0.4, ~0.6, and ~0.8, respectively. These images were color-coded to delineate the local curvature (κ) along the projected contours of the NDs (fig. S4) (*22*). Further analysis revealed a consistent curvature variation profile across different particle shapes, transitioning smoothly from positive in the head regions to negative at the waist (fig. S5). Additionally, within the convex head regions, the corners tended to exhibit higher local curvature compared to the caps. Despite differences in concavity, all of the NDs exhibited self-complementarity in local curvature, which would be crucial for promoting directional interparticle interactions. The concave waist acted as a natural binding site, recognizing and interlocking with the convex head of another ND (Fig. 1E), akin to a lock-and-key process (*23*).

ND self-assembly and superlattice formation

This concave-convex curvature fitting promoted specific and stable bonding between NDs, with the bond directionality flexibly adjustable through modulation of the local curvature. To quantify the orientation between two interlocked NDs, we introduced the alignment angle (θ), defined as the angle between the extensions of their longitudinal axes. This angle reflects how NDs aligned themselves to achieve optimal curvature matching during the self-assembly process.

To explore how concavity affects local particle packing, we dried a dilute hexane solution of NDs onto TEM grids and examined the pairing configurations of interlocked NDs. We identified three primary concave-convex fitting modes in ND pairs (Fig. 1F). High-concavity NDs ($d/D < 0.55$), exemplified by ND-1, favored a corner-fitting mode (fig. S6A), in which the corner of one ND fit tightly into the waist of another, forming parallel pairs with an offset in positioning. Conversely, low-concavity NDs ($d/D > 0.65$), such as ND-3, predominantly adopted a cap-fitting configuration (fig. S6C), where the cap region engaged with the waist of another ND. For NDs with moderate concavity ($0.55 < d/D < 0.65$), represented by ND-2, although corner fitting was still observed, they tended to adopt a hybrid-fitting mode (fig. S6B), involving both corner and cap regions to achieve curvature matching with neighboring NDs. These locally favored pairing configurations were primarily dictated by the degree of geometric complementarity between interlocked NDs, which tended to maximize contact between their convex and concave regions.

We hypothesized that by adjusting the concavity of NDs, we could fine-tune particle bonding directionality and thus program the structure

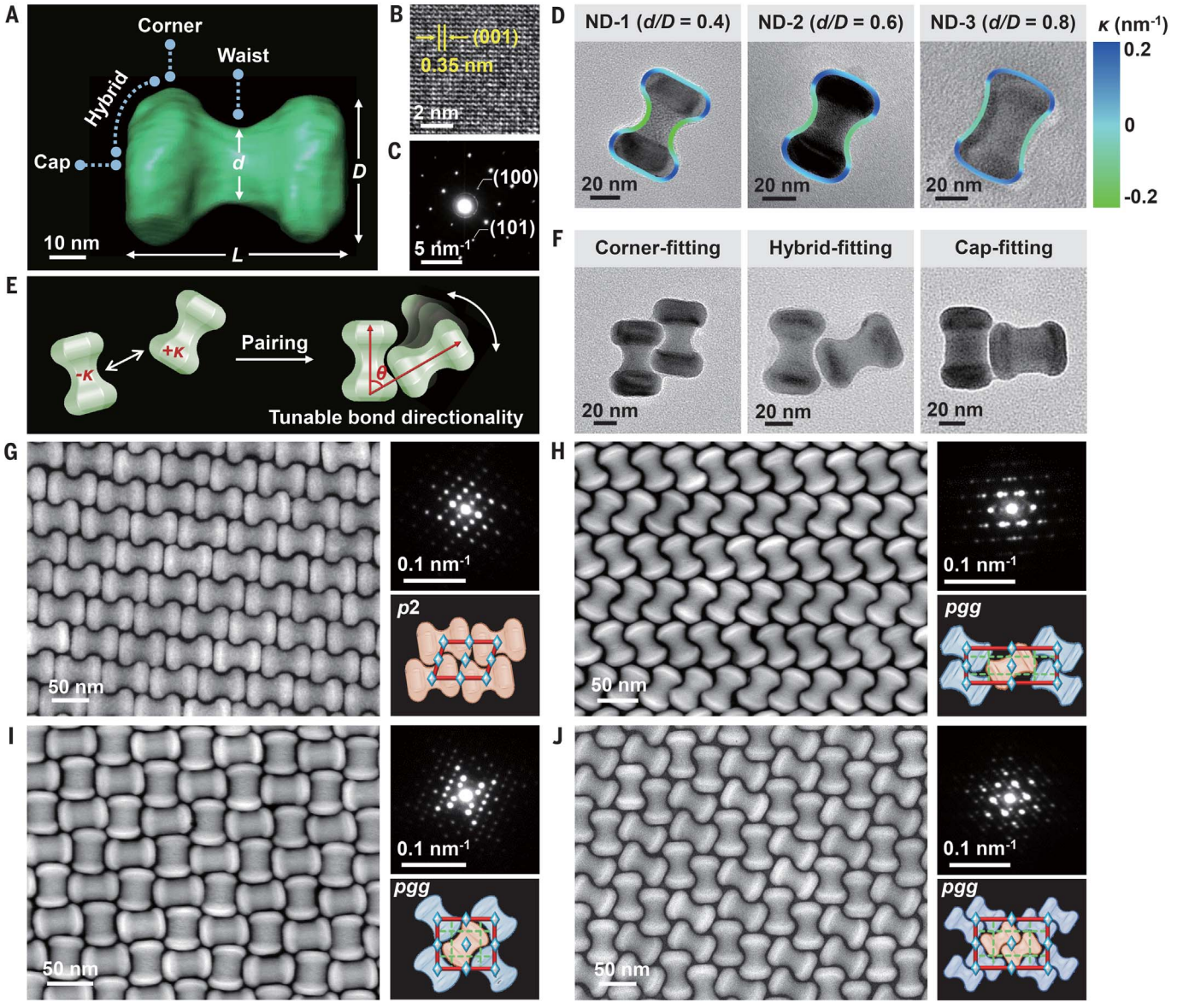

Fig. 1. Engineering the structure of 2D ND superlattices through local curvature modulation. (**A** to **C**) Structural characterization of a single ND: (A) 3D structural reconstruction, (B) HRTEM image, and (C) WAED pattern. (**D**) TEM images of NDs with three representative concavities, with their projected contours color-coded to indicate variations in local curvature (κ). (**E**) Schematic illustrating how NDs pair up through concave-convex curvature fitting, with adjustable alignment angles via curvature modulation. (**F**) TEM images of paired NDs, showing three distinct concave-convex fitting modes between NDs, dictated by their concavity. (**G** to **J**) HAADF-STEM images, SAED patterns (top right), and structural models (bottom right) of various 2D superlattices: (G) parallel, (H) herringbone, (I) chevron, and (J) bi-chevron. The structural models indicate the symmetry of the respective lattice, with different colors representing different particle orientations.

of the resulting superlattices, provided that extended interlocking assembly of NDs was achievable. To test this hypothesis, we performed self-assembly by drop-casting a hexane solution containing NDs onto the surface of a subphase such as diethylene glycol (DEG) (*24*), followed by controlled solvent evaporation (fig. S7). This method allowed NDs to assemble while lying flat at the liquid-air interface.

However, achieving long-range ordered assembly of NDs remained a substantial challenge (*25*). The primary obstacle stemmed from the steric hindrance associated with nonconvex particles, where NDs could become irreversibly locked by their neighbors before reaching equilibrium. Indeed, our initial attempts often resulted in kinetically arrested aggregates characterized by disorder or only short-range order (fig. S8). To overcome this, we exploited depletion interactions by introducing an excess of oleic acid into the ND solution. These free oleic acid molecules served as depletants, progressively inducing specific attraction between adjacent NDs as the solvent evaporated (fig. S9) (*26*, *27*).

This strategy proved highly effective in mitigating kinetic arrest and promoting the extended interlocking of NDs (fig. S8), resulting in large-area superlattice membranes upon complete solvent evaporation. Figure 1, G to J, present high-angle annular dark-field scanning TEM (HAADF-STEM) images of 2D superlattices with varying structural complexities, assembled from NDs with different concavities. Analysis of these distinct superlattices revealed

a common characteristic in their local packing: Each ND provided two binding sites at its waist for interlocking with two neighboring NDs, while its two heads simultaneously engaged with the waists of two adjacent NDs. This intricate arrangement led to a globally interlocked architecture with excellent translational order, as confirmed by small-angle electron diffraction (SAED).

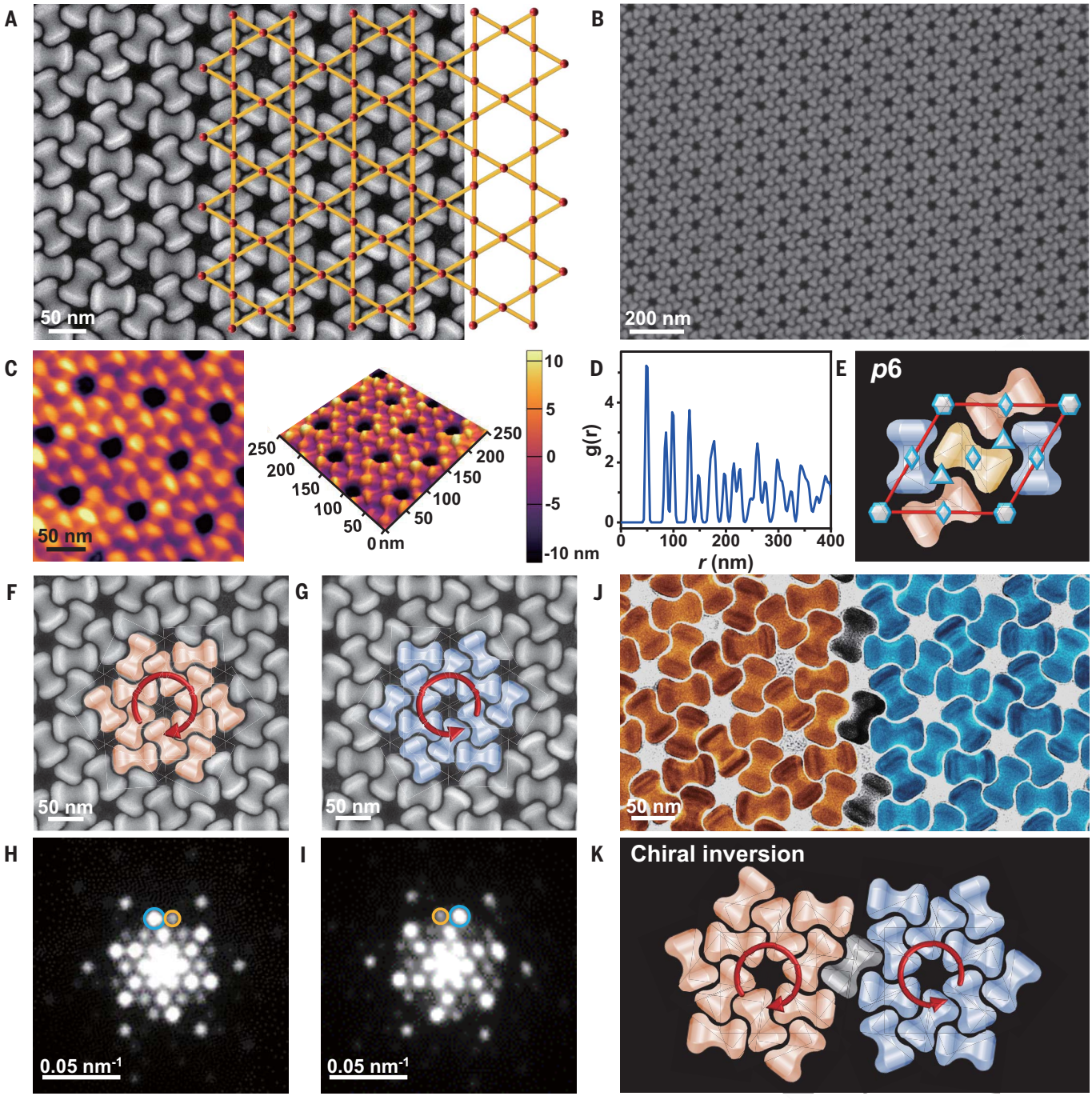

Fig. 2. Chiral Kagome lattices self-assembled from moderate-concavity NDs. (**A** to **E**) Structural characterization of Kagome lattices: (A) HAADF-STEM image, (B) SEM image, (C) AFM image and corresponding 3D topography view on the right, (D) radial distribution function computed from TEM images, and (E) structural model showing the *p*6 symmetry. The orange lines connecting the centroids (red dots) of NDs in (A) illustrate the trihexagonal motif, characteristic of the Kagome lattice. (**F** to **I**) Planar chirality of Kagome lattices: (F and G) HAADF-STEM images and (H and I) corresponding SAED patterns of two distinct chiral domains of the Kagome lattice. The colored NDs in the HAADF-STEM images highlight the gear-like superstructures formed from ND trimers, which rotate either clockwise (F) or counterclockwise (G) as indicated by the red arrows. The asymmetric diffraction spots (indicated by blue and orange circles) in the SAED patterns indicate opposite handedness of the two domains. (**J**) False-colored TEM image, showing the boundary between two distinct chiral domains of the Kagome lattice. (**K**) Schematic illustrating chiral inversion between two adjacent domains, facilitated by a single ND (colored gray) at the boundary.

Further examination showed that the locally favored pairing configurations of NDs were largely maintained in the resulting superlattices, with their structure strongly influenced by the concavity of NDs. Specifically, high-concavity NDs (d/D < 0.55) naturally arranged into extended rows (fig. S10), where the corners of each ND fit snugly into the waists of neighboring particles. This packing motif manifested in two distinct tessellation patterns, shaped by the local curvature of the cap regions in NDs. For NDs with flat caps, such as ND-1, the rows of interlocked ND3s tended to align unidirectionally, forming parallel lattices characterized by *p*2 wallpaper symmetry (Fig. 1G and fig. S11). This low-symmetry lattice was further stabilized by cap-to-cap interactions between NDs in adjacent rows. However, when the caps of NDs were more rounded, neighboring ND rows tended to alternate in orientation to create a zigzag pattern, resulting in herringbone lattices with *pgg* symmetry (Fig. 1H and fig. S12).

By contrast, the self-assembly of low-concavity NDs (d/D > 0.65) resulted in the formation of chevron lattices (Fig. 1I and fig. S13). These densely packed lattices, featuring *pgg* symmetry, were characterized by a V-shaped packing motif formed from two NDs interlocking through cap fitting. A notable feature of chevron lattices was the flexibility in adjusting the alignment angle between neighboring NDs without altering lattice symmetry (fig. S14). This tunability was achieved by varying the aspect ratio (L/D) of NDs, with the alignment angle decreasing as the aspect ratio increased to maintain dense packing (fig. S15). For instance, the self-assembly of ND-3 with an aspect ratio of 1.5 led to a nearly orthogonal arrangement with an alignment angle of 86° (Fig. 1I), whereas a smaller alignment angle of 69° was observed when assembling NDs with a higher aspect ratio of 1.9 (fig. S14).

When moderate-concavity NDs (0.55 < d/D < 0.65) were used for self-assembly, more complex structures could be anticipated because of their tendency for hybrid fitting, which allowed for greater flexibility in tuning particle bonding. A more complex structure was illustrated by the formation of bi-chevron lattices from ND-2 (Fig. 1J and fig. S16). These close-packed lattices displayed an exotic pattern with *pgg* symmetry, in which two pairs of parallel NDs served as a repeating unit, tessellating similarly to chevron lattices. However, unlike chevron lattices, each ND in the bi-chevron lattice participated in dual pairing configurations—hybrid fitting and corner fitting—with three neighboring NDs. This packing behavior aligned with the two locally preferred fitting modes observed in moderate-concavity NDs (fig. S6B), resulting in a unit cell consisting of four NDs aligned in two orientations. The alignment angle between hybrid-fitting NDs was ~62°, as confirmed by WAED analysis (fig. S17).

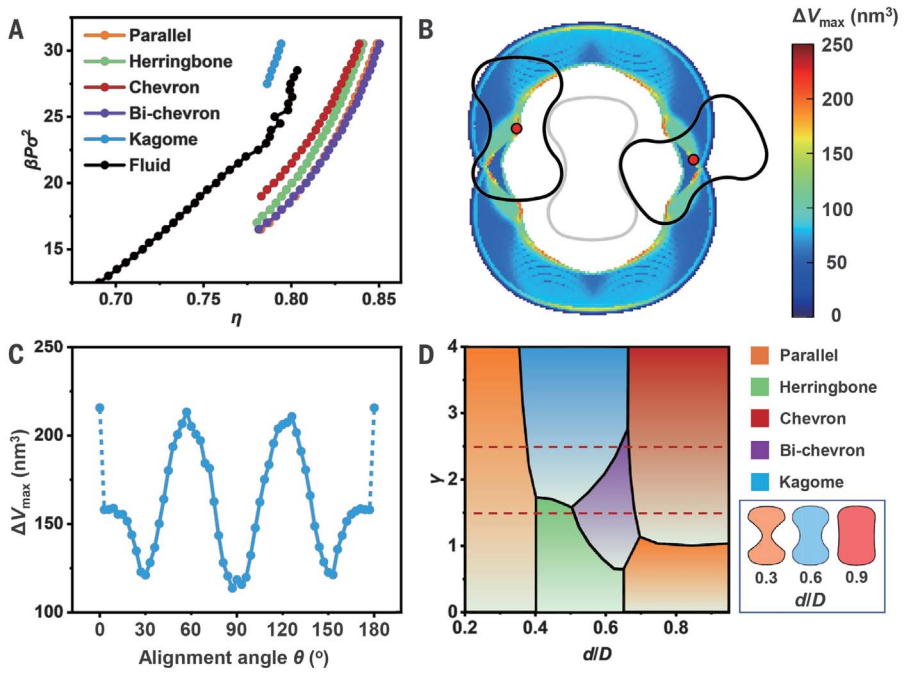

Fig. 3. Formation mechanism of Kagome lattices. (**A**) EOS of the hard-core system of ND-2, derived from simulations. Colored lines represent the expansion results for various perfect crystal structures, while the black line represents the compression of random fluid states. (**B**) Calculated ΔV_{max} for ND pairs under various particle orientations, plotted as a function of relative particle position. The two favored pairing configurations that maximize ΔV_{max} are highlighted with black NDs to indicate the optimal orientations. (**C**) Calculated ΔV_{max} for ND pairs under various particle positions, plotted as a function of relative particle orientation. (**D**) Phase diagram illustrating the phase behaviors of NDs with varying d/D ratios. The region between the two dashed lines represents the predicted phases when γ ranges from 1.5 to 2.5.

Kagome lattices

The versatility of moderate-concavity NDs in constructing complex architectures was further demonstrated by the formation of Kagome lattices (Fig. 2 and fig. S18). The Kagome lattice, known for its distinctive 2D arrangement of interconnected triangles, hexagons, and voids, has attracted interest because of its specific geometric and topological properties (*28*). Although Kagome lattices have been observed previously through NC self-assembly (*29*, *30*), the resulting lattices were often low in quality or exhibited structural distortion. Here, by using moderate-concavity NDs, we achieved large-area, high-quality Kagome lattices with minimal structural defects. Figure 2A shows the HAADF-STEM image of Kagome lattices self-assembled from ND-2, the same particles used for forming bi-chevron lattices. Connecting the centroids of individual NDs led to a trihexagonal pattern featuring three distinct particle orientations and periodic voids, aligning with the geometric characteristics of a Kagome lattice. These features were further confirmed by scanning electron microscopy (SEM, Fig. 2B) and atomic force microscopy (AFM, Fig. 2C).

The self-assembly of Kagome lattices could be reliably achieved by using various moderate-concavity NDs (fig. S19), indicating the robustness of this assembly approach. Kagome lattices often coexisted with the dense bi-chevron lattices (fig. S20), despite having a much lower packing efficiency (~65%, fig. S21). Moreover, single domains of Kagome lattices could extend up to several micrometers in lateral size (fig. S18), suggesting that their formation was under thermodynamic control. The long-range translational order of Kagome lattices was further supported by the radial distribution function (Fig. 2D and fig. S22) and grazing incidence small-angle x-ray scattering (GISAXS, fig. S23) (*31*).

Further analysis revealed that the Kagome lattice displayed *p*6 symmetry (Fig. 2E), with each ND interlocking with its four nearest neighbors through hybrid fitting. This arrangement led to the formation of two vertex-sharing trimers, with an alignment angle of 60° between adjacent NDs (fig. S24). These trimers were essential for creating the Kagome pattern, as the trihexagonal motif emerged when six adjacent trimers oriented to form a gear-like superstructure (Fig. 2, F and G). Notably, these h3ierarchical superstructures were observed to rotate either clockwise (Fig. 2F) or counterclockwise (Fig. 2G), suggesting the development of planar chirality.

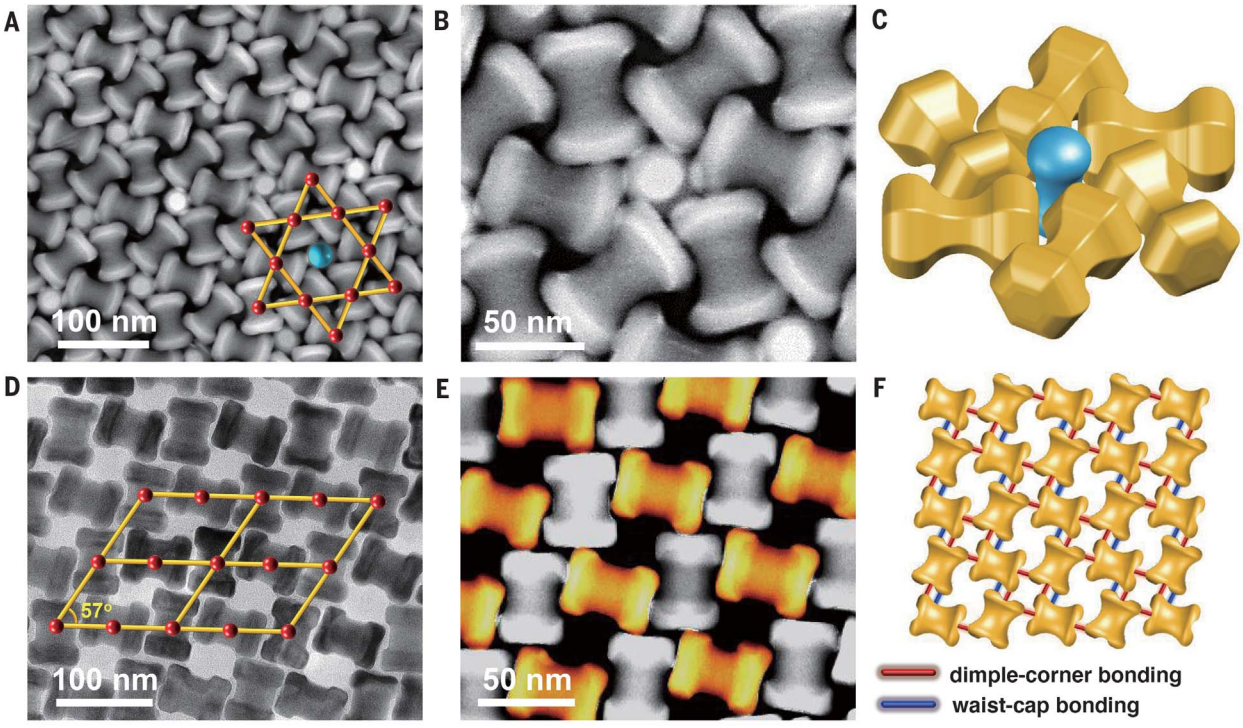

Fig. 4. Self-assembly of NDs into complex superlattices by design. (**A** to **C**) Characterization of AB_3-type binary superlattices self-assembled from two types of NDs: (A) HAADF-STEM image, (B) high-magnification HAADF-STEM image, and (C) structural schematic illustrating the arrangement of large and small NDs. The orange lines connecting the centroids (red dots) of the large NDs in (A) depict the trihexagonal motif, with the smaller ND (blue dot) occupying the void. (**D** to **F**) Characterization of open oblique lattices self-assembled from NDs though multivalent bonding interactions: (D) TEM image, (E) false-colored HAADF-STEM image, and (F) structural schematic highlighting the bonding configurations of individual NDs. The orange lines connecting the centroids (red dots) of NDs in (D) depict the oblique lattice. Half of the NDs in (E) are colored in orange to illustrate their distinct bonding configurations compared to the uncolored NDs.

This chirality was further supported by the reciprocal space analysis (*32*, *33*), in which the diffraction spots in the SAED patterns displayed clear asymmetry in intensity (Fig. 2, H and I). The as-assembled Kagome lattice was a racemic mixture, comprising domains of both left and right handedness, which was expected given the achiral nature of NDs. An interesting observation was that at the boundary between two chiral domains, a single row of NDs was often present (Fig. 2J). These NDs, as an integral component of one domain, smoothly inverted the chirality of adjacent domains by engaging in corner fitting with NDs in the other domain (Fig. 2K). Increasing the concentration of NDs could lead to the formation of bilayer or trilayer Kagome lattices (fig. S25), with each layer maintaining consistent handedness. An interlayer offset was observed to ensure geometric complementarity between NDs across different layers (fig. S25 and S26).

Formation mechanism

The Kagome lattice, among the various superlattices observed in our experiments, likely represents the most intriguing phase, given its distinctive tessellation patterns and low packing efficiency. Previous studies on Kagome lattices assembled from triblock patchy particles suggested that vibrational entropy played a pivotal role in stabilizing these non–close-packed structures (*34*). To understand the formation mechanism of Kagome lattices assembled from NDs, we first investigated whether they could form through a purely entropy-driven process involving hard particles. To this end, we performed isobaric-isothermal floppy-box Monte Carlo (*NPT* FBMC) simulations based on a system of 960 particles, using shape parameters measured from ND-2 (supplementary text 1) (*35*, *36*). Starting from experimentally observed candidate crystal structures, including parallel, herringbone, chevron, bi-chevron, and Kagome lattices, as well as disordered fluids, we derived the equation of state (EOS) of the corresponding system.

The results indicated that, among these crystal structures, the Kagome lattice was the least favorable phase, with its packing density (η) even lower than that of glassy fluids (Fig. 3A). These findings suggested that purely hard-core interactions between NDs were insufficient to stabilize the Kagome lattice. Given these results, we proposed that depletion interactions, which were intentionally introduced during self-assembly to overcome kinetic trapping, played a crucial role in stabilizing the Kagome lattice. We hypothesized that the depletion effect enhanced attractive interactions between concave and convex regions of adjacent NDs, guiding them into the specific arrangements needed to form the Kagome lattice. To validate this hypothesis, we conducted further calculations to examine whether depletion interactions could indeed stabilize the Kagome lattice.

The depletion attraction between two particles was proportional to both the overlapping exclusion volume (ΔV) and the number density of depletant (free oleic acid molecules) in solution (*23*). For any two surfaces, the interaction range was determined by twice the radius (r_{dep}) of the depletant molecules. To investigate the effect of depletion interactions on the local packing of NDs, we calculated ΔV for a pair of interacting NDs using a 3D particle model (supplementary text 2), with shape parameters obtained from ND-2. We sampled the local maximum ΔV (ΔV_{max}) across various particle orientations and positions using the direct Monte Carlo method. Figure 3B presents the depletion interaction landscape, represented by ΔV_{max} for various particle orientations. Notably, ΔV_{max} increased substantially when two NDs engaged in corner-fitting and hybrid-fitting modes, consistent with the two locally preferred pairing configurations observed for ND-2 (fig. S6B).

These findings suggested that during self-assembly, NDs tended to adopt concave-convex fitting modes that maximize ΔV_{max}. This mechanism was further supported by plotting ΔV_{max} across various particle positions against alignment angles, which revealed that the depletion interaction peaked at $\theta = 0°$ and nearly at $\theta = 60°$ (Fig. 3C). The calculated ΔV_{max} values for the corner-fitting and hybrid-fitting configurations, referred to as ΔV_{corner} and ΔV_{hybrid}, were ~216 and ~205 nm^3, respectively, assuming $r_{dep} = 0.75$ nm for the depletant molecules (*37*).

To further explore how depletion interactions influenced the formation of specific superlattices, we calculated the total overlapping exclusion volume (ΔV_{tot}) for individual NDs within a lattice. As an approximation, ΔV_{tot} could be considered as the sum of several local ΔV_{max} values, determined by the lattice structure and curvature-fitting modes. In the Kagome lattice, each ND interacted through hybrid fitting with four nearest neighbors (fig. S27A), thus making ΔV_{tot} approximated as four times ΔV_{hybrid}, or 820 nm^3. In the bi-chevron lattice, each ND coordinated with two nearest neighbors through hybrid fitting and one nearest neighbor through corner fitting (fig. S27B), resulting in ΔV_{tot} equal to $2\Delta V_{hybrid} + \Delta V_{corner}$, or 626 nm^3. These calculations suggested that at sufficiently high depletant concentrations, the system favored the Kagome lattice because of its stronger depletion interactions. By contrast, the bi-chevron lattice was entropically more favorable because of its higher packing density. This dual preference accounted for the frequent coexistence of these two phases within the same system.

These calculations focused on moderate-concavity NDs, but we speculated that curvature-guided depletion interactions similarly governed the extended assembly of both low- and high-concavity NDs (fig. S8). During solvent evaporation, the progressively increasing depletion interaction strengthened the binding between the concave and convex regions of neighboring NDs, allowing them to recognize and adjust their orientations for optimal concave-convex contact. This process not only helped avoid kinetic traps but also facilitated the global interlocking of NDs into the corresponding superlattice structures. Concurrently, lateral capillary forces could further enhance the concave–convex attractions at the later stage of evaporation (*38*, *39*), bringing NDs into closer proximity. As evaporation continued, van der Waals interactions between the surface ligands of adjacent NDs became increasingly dominant, effectively locking the particles in place once the solvent had fully evaporated (*40*). This transition solidified the as-assembled superlattices, ensuring their structural integrity during transfer from the liquid surface to various substrates.

Phase behavior

To construct a comprehensive phase diagram, we introduced a phenomenological parameter γ, which served to describe the relative strength of concave-convex interactions compared to convex-convex or concave-concave interactions between two NDs (supplementary text 3). This parameter reflects the degree of compatibility of local curvatures between the concave and convex patches on neighboring particles, with higher γ values indicating stronger interparticle concave-convex attractions. We investigated the system using a 2D particle model with shape parameters based on ND-2, while continuously varying the concavity (d/D ratio) from 0.20 to 0.95. Although this particle model was more coarse-grained compared to the one used for depletion calculations, it allowed us to construct a phase diagram that qualitatively captured the phase behaviors of differently shaped NDs (Fig. 3D).

By comparing the various lattice structures predicted by the phase diagram with experimental results, we estimated γ to fall within the range of 1.5 to 2.5. Within this range, the Kagome lattice could form and coexist with the bi-chevron lattice when the d/D ratio ranged from ~0.55 to ~0.65 (fig. S28), which agreed well with experimental observations. Additionally, the phase diagram predicted that for NDs with very narrow waists (e.g., $d/D = 0.3$), the stable phase was the parallel lattice, whereas for NDs with very wide waists (e.g., $d/D = 0.9$), the stable phase was the chevron lattice. These predictions were supported by experiments (fig. S29), reinforcing the validity of this phase diagram in predicting the structural outcome of superlattices assembled from NDs.

Binary superlattices and low-density superlattices

The established mechanism of curvature-guided depletion was critical, as it opened up new possibilities for creating sophisticated architectures that are otherwise unattainable with convex building blocks. For example, coassembling two types of NDs with differing dimensions led to the formation of AB_3-type binary superlattices (fig. S30). In this close-packed structure, the large NDs interlocked to form a chiral Kagome pattern (Fig. 4A), while the smaller NDs occupied the voids (Fig. 4B). To achieve optimal local curvature matching, each smaller ND aligned vertically, positioning its waist to interact with the corners of six adjacent larger NDs (Fig. 4C). Incorporating particles into the periodic voids of the Kagome lattice introduced an additional level of structural complexity, which might lead to the emergent properties stemming from the distinctive topological arrangement of the lattice (*30*, *41*).

The versatility of this curvature-guided design principle was further demonstrated by its ability to direct the assembly of low-symmetry, low-density lattices. These lattices were achieved by introducing multivalent bonding interactions through the creation of additional concave features into NDs. As a proof of concept, we synthesized NDs with two small dimples at their endcaps by modifying the reaction conditions (fig. S31). Along with the regular binding sites at the waist, these dimples provided additional sites that selectively bound with the high-convex corners of neighboring NDs through local curvature matching. This dual concave-convex interaction mode led to symmetry breaking, resulting in the formation of an open oblique lattice with an internal angle of 57° (Fig. 4D). In this low-symmetry lattice, the concave waists and dimples of half the NDs fully engaged in interlocking, whereas the other half remained uncoordinated at their waists (orange NDs in Fig. 4E). This approach led to a packing fraction of ~59% (fig. S32), which was even lower than that of the Kagome lattice. The multiple specific bonding interactions between neighboring NDs were likely responsible for stabilizing this unusual open lattice (Fig. 4F).

Conclusions

Our study demonstrates that the curvature of nonconvex NCs can be leveraged to program directional interparticle interactions. By engineering the local curvature of NDs, we achieved precise and flexible control over particle bonding directionality, enabling the formation of diverse and intricate 2D superlattices. Our research also highlights the critical role of curvature-guided depletion interactions, which not only facilitated the global interlocking of NDs but also stabilized open structures such as Kagome lattices. With interlocked configurations and tunable lattice symmetry, these ND superlattices could have distinctive mechanical and optical properties. Additionally, this curvature-mediated design principle could serve as a general strategy for guiding the self-assembly of various nonconvex NCs (*42*). Although this work primarily focused on single-component superlattices, it paves the way for creating more complex multicomponent superlattices by coassembling NDs with appropriately shaped convex NCs.

REFERENCES AND NOTES

1. C. L. Bassani *et al.*, *ACS Nano* **18**, 14791–14840 (2024).
2. L. Cademartiri, K. J. M. Bishop, *Nat. Mater.* **14**, 2–9 (2015).
3. M. R. Jones *et al.*, *Nat. Mater.* **9**, 913–917 (2010).
4. M. Liu, X. Zheng, V. Grebe, D. J. Pine, M. Weck, *Nat. Mater.* **19**, 1354–1361 (2020).
5. K. Deng, Z. Luo, L. Tan, Z. Quan, *Chem. Soc. Rev.* **49**, 6002–6038 (2020).
6. Z. Xue, C. Yan, T. Wang, *Adv. Funct. Mater.* **29**, 1807658 (2019).
7. M. A. Boles, M. Engel, D. V. Talapin, *Chem. Rev.* **116**, 11220–11289 (2016).
8. X. Li, X. Liu, X. Liu, *Chem. Soc. Rev.* **50**, 2074–2101 (2021).
9. L. Z. Zornberg *et al.*, *ACS Nano* **17**, 3394–3400 (2023).
10. M. S. Lee, D. W. Yee, M. Ye, R. J. Macfarlane, *J. Am. Chem. Soc.* **144**, 3330–3346 (2022).

11. R. J. Macfarlane, M. N. O'Brien, S. H. Petrosko, C. A. Mirkin, *Angew. Chem. Int. Ed.* **52**, 5688–5698 (2013).
12. W. Zhou, Y. Li, B. E. Partridge, C. A. Mirkin, *Chem. Rev.* **124**, 11063–11107 (2024).
13. J. Park *et al*., *Nat. Mater.* **3**, 891–895 (2004).
14. X. Ye *et al*., *Proc. Natl. Acad. Sci. U.S.A.* **107**, 22430–22435 (2010).
15. A. Kim *et al*., *ACS Nano* **18**, 939–950 (2024).
16. C. Yi *et al*., *Science* **369**, 1369–1374 (2020).
17. Z. Miao, C. Y. Zheng, G. C. Schatz, B. Lee, C. A. Mirkin, *Angew. Chem. Int. Ed.* **60**, 19035–19040 (2021).
18. H. Chen *et al*., *Nature* **599**, 222–228 (2021).
19. M. Qi *et al*., *J. Am. Chem. Soc.* **145**, 2739–2744 (2023).
20. Q. Chen, S. C. Bae, S. Granick, *Nature* **469**, 381–384 (2011).
21. S. Wan *et al*., *ACS Nano* **16**, 21315–21323 (2022).
22. D. A. Walker, E. K. Leitsch, R. J. Nap, I. Szleifer, B. A. Grzybowski, *Nat. Nanotechnol.* **8**, 676–681 (2013).
23. S. Sacanna, W. T. Irvine, P. M. Chaikin, D. J. Pine, *Nature* **464**, 575–578 (2010).
24. A. Dong, J. Chen, P. M. Vora, J. M. Kikkawa, C. B. Murray, *Nature* **466**, 474–477 (2010).
25. Y. Liu *et al*., *Chem. Sci.* **11**, 4065–4073 (2020).
26. K. Zhao, T. G. Mason, *Rep. Prog. Phys.* **81**, 126601 (2018).
27. E. Marino, Z. Jiang, T. E. Kodger, C. B. Murray, P. Schall, *Langmuir* **39**, 12533–12540 (2023).
28. J. L. Atwood, *Nat. Mater.* **1**, 91–92 (2002).
29. Y. Taniguchi *et al*., *ACS Nano* **11**, 9312–9320 (2017).
30. Z. Li *et al*., *Sci. Adv.* **10**, eadp3756 (2024).
31. N. Mac Fhionnlaoich, R. Qi, S. Guldin, *Langmuir* **35**, 16605–16611 (2019).
32. K. Zhao, T. G. Mason, *J. Phys. Condens. Matter* **26**, 152101 (2014).
33. H. Deng *et al*., *Nature* **632**, 775–781 (2024).
34. X. Mao, Q. Chen, S. Granick, *Nat. Mater.* **12**, 217–222 (2013).
35. J. de Graaf, L. Filion, M. Marechal, R. van Roij, M. Dijkstra, *J. Chem. Phys.* **137**, 214101 (2012).
36. D. Frenkel, B. Smit, *Understanding Molecular Simulation: From Algorithms to Applications* (Elsevier, 2001).
37. S. N. Hosseini *et al*., *Adv. Funct. Mater.* **30**, 2005491 (2020).
38. N. Bowden, F. Arias, T. Deng, G. M. Whitesides, *Langmuir* **17**, 1757–1765 (2001).
39. P. J. Yunker, T. Still, M. A. Lohr, A. G. Yodh, *Nature* **476**, 308–311 (2011).
40. F. Zhang, R. Liu, Y. Wei, J. Wei, Z. Yang, *J. Am. Chem. Soc.* **143**, 11662–11669 (2021).
41. X. Wu, D. Chakraborty, A. P. Schnyder, A. Greco, *Phys. Rev. B* **109**, 014517 (2024).
42. Q. Chen, Y. Jia, S. Xie, Z. Xie, *Chem. Soc. Rev.* **45**, 3207–3220 (2016).

ACKNOWLEDGMENTS

Funding: This work was supported by National Key Research and Development Program of China (2022YFA1503501), NSFC (52333013, 22025501, 22088101, 52202088, 52373204, 52394272, 224B1019), Science and Technology Commission of Shanghai Municipality (24TS1410200, 23JC1400100, 2024ZDSYS02, 24JD1400700), Shanghai International Science and Technology Partnership Project (23520750400), China Postdoctoral Science Foundation (2024M760493), and the Fundamental Research Funds for the Central Universities (20720220010). T.L. was supported by the Shanghai Rising-Star Program (24QA2700800). R.N. was supported by the Academic Research Fund from the Singapore Ministry of Education (RG151/23 and MOE2019-T2-2-010) and the National Research Foundation, Singapore, under its 29th Competitive Research Program (CRP) Call (NRF-CRP29-2022-0002). **Author contributions:** A.D. and T.L. conceived and supervised this work. S.W. performed the experiments and data analysis. X.X. and R.N. conducted the MC simulations and depletion interaction calculations. J.L. performed phase diagram constructions. Y.G., H.Z., and F.W. contributed to ND synthesis. Z.Z. conducted AFM characterization. X.W. and D.Y. contributed to geometric calculation and analysis. All authors participated in the writing and revision of the manuscript. **Competing interests:** The authors declare no competing interests. **Data and materials availability:** All data are available in the main text or the supplementary materials.

SUPPLEMENTARY MATERIALS

science.org/doi/10.1126/science.adu4125
Materials and Methods
Supplementary Text
Figs. S1 to S33
References (*43*–*45*)
Movie S1

Submitted 6 November 2024; accepted 9 January 2025
10.1126/science.adu4125

Curvature-guided depletion stabilizes Kagome superlattices of nanocrystals

Siyu Wan, Xiuyang Xia, Yutong Gao, Heyang Zhang, Zhebin Zhang, Fangyue Wu, Xuesong Wu, Dong Yang, Tongtao Li, Jianfeng Li, Ran Ni, and Angang Dong

Science **387** (6737), . DOI: 10.1126/science.adu4125

Editor's summary

Adjusting the curvature of dumbbell-shaped nanocrystals can control particle bonding directionality to form a variety of intricate two-dimensional superlattices. Wan *et al*. found that superlattice formation from these rare earth fluoride colloids results from globally interlocking self-assembly driven by curvature-guided depletion interactions that are difficult to achieve with conventional convex particles (see the Perspective by Korgel). This method could also stabilize structures with periodic vacancies, such as the chiral Kagome lattice. —Phil Szuromi